European Spine Journal (2019) 28:633–648
https://doi.org/10.1007/s00586-019-05903-8

ORIGINAL ARTICLE

A histocytological and radiological overview of the natural history of intervertebral disk: from embryonic formation to age-related degeneration

Feng Wang[1,2] · Cong Zhang[1,2] · Arjun Sinkemani[1,2] · Rui Shi[1,2] · Zhi-Yang Xie[1,2] · Lu Chen[1,2] · Lu Mao[1,2] · Xiao-Tao Wu[1,2]

Received: 2 April 2018 / Revised: 5 January 2019 / Accepted: 25 January 2019 / Published online: 4 February 2019

Abstract

Purpose To elucidate the natural history of intervertebral disk (IVD) and characterize its embryonic beginnings and age-related degeneration.

Methods Coronal sections of embryonic (E13.5-neonatal) and postnatal (4–60-week-old) Sprague–Dawley rat IVD were stained by a series of histological stainings (hematoxylin and eosin, Alcian blue, Picrosirius red, Masson, Periodic acid–Schiff). Growth kinetics within embryonic IVD were evaluated by immunohistochemical staining of Ki67 and proliferating cell nuclear antigen. Postnatal maturation and degeneration of IVD were visualized on radiology by X-ray, CT, and MR imaging.

Results During the formation of rat IVD, inner annulus fibrosus (AF) and cartilaginous endplate (CEP) shared similar cell density, extracellular matrix, and potential of growth kinetics; notochord provided increased and enlarged cytoplasmic vacuoles to generate nucleus pulposus (NP), part of which was retained within CEP. Postnatally, vacuolated notochord cells were reduced by devacuolation, while chondrocytic NP cells increased; cartilaginous layers of CEP were narrowed by vertebrae growth and secondary ossification; fibrotic portion of AF decreased as cartilaginous matrix accumulated and infiltrated outward. In aged and degenerated IVD, large longitudinal fissures were detected near the boundaries between inner and outer AF, whereas both reduced cellularity and accumulated cell clusters were evident within the dehydrated NP; only part of these histocytological changes could be reported on radiology.

Conclusions By showing that the natural history of IVD is orchestrated by a dynamic histocytological regulation, our study may facilitate better understanding of the developmental defects, cellular heterogeneity, age-related degenerative mechanisms, and biological regeneration of IVD.

Graphical abstract

These slides can be retrieved under Electronic Supplementary Material.

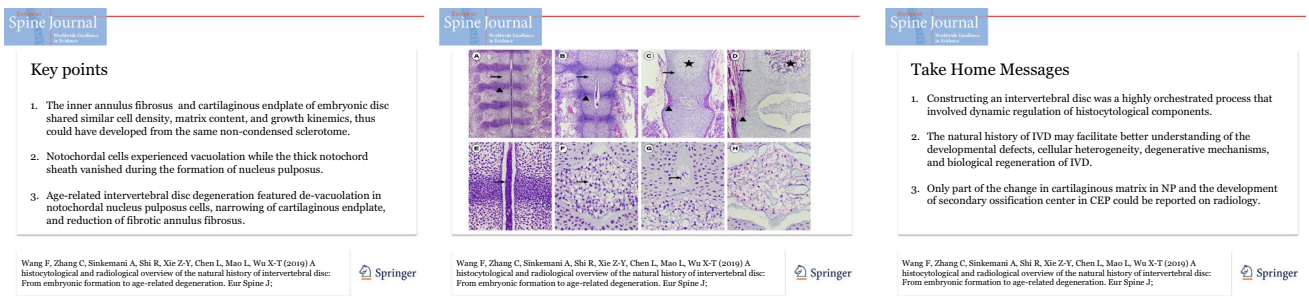

Electronic supplementary material The online version of this article (https://doi.org/10.1007/s00586-019-05903-8) contains supplementary material, which is available to authorized users.

Extended author information available on the last page of the article

Keywords Intervertebral Disk · Embryogenesis · Cytoplasmic Vacuole · Notochord · Sclerotome

Introduction

The intervertebral disk (IVD) is the fundamental building block of the spine, connecting adjacent vertebrae, absorbing mechanical loading, and maintaining a motional segment that allows flexion, extension, bending, and rotation [1]. A young and normal disk is composed of an inner, gelatinous nucleus pulposus (NP), an outer, concentric annulus fibrosus (AF), and a capping cartilaginous endplate (CEP) that is anchored into the growth plate of the vertebral body [2]. A degenerated IVD, which often features histologically deteriorating components and compromised biomechanics [3], has long been noted as a major etiological factor in the world's most disabling condition, low back pain [4]. Although endoscopic discectomy now provides minimally invasive approaches for rapid symptom relief [5–7], it remains challenging to reverse, by surgery, the pathogenic basis that underlies IVD degeneration (IVDD) [2, 3]. Thus, astronomical sums have been spent globally in various areas of basic research, in an endeavor to understand what precipitates and promotes degenerative changes within the IVD [8].

Traditionally, IVDD appears on magnetic resonance imaging (MRI) scans as a disk that reduces T2-weighted signals [9, 10]. Based on this classification, an increasing number of pathological factors and susceptibility genes relating to degenerative disks have been identified [3, 11]. To date, identified promoters of IVDD include older age, acute injuries, unphysiological biomechanics, oxidative stress, diabetes, smoking, obesity, and genetic factors [2, 3, 11]. However, because radiological findings do not always include histopathological changes [10], association studies addressing the pathogenesis of IVDD have yielded inconsistent and even conflicting results, raising concerns about whether all such radiologically degenerative disks are histologically, or on molecular basis, degenerated [8]. This controversy has been fueled in recent years by accumulating evidence that (1) "degenerative" disks with reduced T2 signal intensity are common in adolescents [12]; (2) nearly 21% of multilevel IVDD cases showed "skipped level" patterns, whereby apparently healthy disks are located between degenerative ones [13]; and (3) some supposedly "degenerative" disks remain silent for years, and no further progression occurs [14]. Presumably, some subgroups of radiologically degenerative disks are dysgenerated during embryogenesis and thus are poorly hydrated from the outset, but still appear normal on radiological scans [8]. To identify these maldeveloped disks and exclude them from the entity of histologically degenerated IVD [8], an overview of the natural history of IVD, detailing its progressing from embryonic formation all the way to age-related degeneration, is needed.

Studies with model organisms have shown that the mammalian NP develops from the axial notochord, whereas the AF and CEP are derived from the paraxial mesoderm [15–20]. However, to date, it is unclear whether there are any critical developmental points, or a histocytological basis by which the generation of a normal IVD could be disrupted. Moreover, because the embryonic map of vertebral column formation varies evolutionarily from teleostean to avian and mammalian embryos [15, 16, 21–24], for example, in zebrafish the notochord rather than the somites secretes bone matrix and generates vertebral bodies [21], while in chickens the somite begins to generate vertebrae but the IVD formed therein lacks a central NP [22], and there is a need to better understand the course of disk development in the mammals used for investigating both degeneration and regeneration of the IVD.

In this study, we explored the natural history of rat IVD, from embryonic formation to age-related degeneration. Here, we show that both the axial notochord and paraxial mesoderm underwent dynamic histocytological changes during the generation of a normal disk, whereas an aged and degenerated IVD featured significant remodeling of both disk cells and extracellular matrix. By showing that construction of the IVD is a sophisticated, orchestrated process involving a dynamic histocytological regulation, our findings may help us to better understand developmental defects, cellular heterogeneity, age-related degeneration, and biological regeneration of the IVD.

Materials and methods

Rat embryos

Animal studies were approved by the Laboratory Animal Care and Use Committee of Southeast University. All experimental rats were treated in accordance with the International Association for the Study of Pain guidelines for the care and use of animals, with the study designed and reported following the ARRIVE (Animal Research: Reporting In Vivo Experiments) guidelines developed by the National Centre for the Replacement Refinement and Reduction of Animals in Research.

To collect rat embryos at different embryonic (E) stages, 20 female (10 weeks old, 200–220 g) and 10 male Sprague–Dawley (SD) rats (10 weeks old, 210–250 g) were allocated into ten mating groups. In each group, one male rat and two female rats were allowed 24 h of free activity and mating, followed by separate housing until labor. The female rats were checked for pregnancy at 12 days post-mating; rats

with positive pregnant signs (increased abdomen circumference and body weight) were deemed to be E11.5 and were used to provide rat embryos, while those without signs of pregnancy were rechecked at 15 days post-mating, with the pregnant animals deemed to be E14.5; non-pregnant animals were allocated to the next round of mating. Rat embryos were collected at E13.5, E14.5, E18.5, and E21.5 (neonatal). At each embryonic stage, the female rats were euthanized with CO_2 and the embryos were isolated, fixed in 4% paraformaldehyde, dehydrated through a graded ethanol series, and embedded in paraffin wax to prepare coronal sections of 3 μm thick.

Postnatal rat spine

IVDs from the postal spine were collected from 4- ($n=4$, 100–110 g), 12- ($n=4$, 200–230 g), 30- ($n=4$, 450–500 g), and 60-week-old ($n=4$, 700–800 g) male SD rats. After euthanization with CO_2, the lumbar (L) spine was harvested and the vertebra–disk–vertebra unit from L3 to L6 was prepared, followed by fixation in 4% paraformaldehyde, decalcification in ethylenediaminetetraacetic solution, dehydration through a graded ethanol series, and embedding in paraffin wax. Coronal sections, 3 μm thick, were prepared. All three IVDs (L3/4, L4/5, and L5/6) were used for the analysis of vacuoles within the NP, while L3/4 and L4/5 were used for the study of age-related changes in the CEP and AF.

Histological staining

Coronal sections were dewaxed in xylene and rehydrated through ethanol to allow HE, Alcian blue, Picrosirius red, Masson, and Periodic acid–Schiff (PAS) staining, according to standard techniques. Briefly, the sections were reacted with Harris hematoxylin for 5 min and eosin for 3 min in HE staining. For Alcian blue and Picrosirius red staining, the sections were reacted for 12 min in Alcian blue (pH 2.5) and for 8 min in Picrosirius red staining solution (G1027 and G1028; Goodbio Ltd., Nanjing, China); the cartilaginous tissues are stained light blue or green by the Alcian blue, while the fibrotic tissue is stained red by the Picrosirius red. For Masson staining (G1006; Goodbio), the rehydrated sections were immersed in Ponceau 2R and acid fuchsin solution for 10 min, phosphomolybdic acid for 5 min, and acidic aniline blue solution for 5 min, without nuclei staining in hematoxylin; collagenous fibers are stained blue, while the myofibers are stained red by Masson staining. For PAS staining (G1008; Goodbio), sections were oxidized in periodic acid for 10 min, reacted with Schiff's reagent for 20 min in the dark, and stained in hematoxylin for 2 min; accumulation of glycoproteins and glycosaminoglycans shows light red staining. Stained disks were visualized under light microscopy (BX41; Olympus, Tokyo, Japan), and images were captured using a digital camera and Q-Capture Pro software (ver. 6.0 Media Cybernetics, Bethesda, MD, USA).

Immunohistochemical staining

After rehydration through graded ethanols, embryonic spine sections were heated to 90 °C for 20 min in sodium citrate buffer (10 mM sodium citrate, PH to 6.0, 0.05% Tween 20) for antigen retrieval, reacted with 3% hydrogen peroxide in methanol to eliminate endogenous peroxidase, blocked with 5% bovine serum albumin in Tris-buffered saline, and incubated with mouse anti-Ki67 (dilution 1:100) (GB13030; Goodbio) or proliferating cell nuclear antigen (PCNA) monoclonal antibodies (dilution 1:200) (ab92552; Abcam PLC, UK) at 4 °C overnight. Binding of the primary antibodies was detected using the Two-Step REAL EnVision+/HRP rabbit/mouse kit (K5007; Dako A/S, Glostrup, Denmark). Briefly, sections were incubated with ChemMate EnVision$^+$/HRP solution for 1 h at room temperature, and the immunoreactivity was visualized with diaminobenzidine for 3 min, which stained the bound primary antibodies brown. Cell nuclei were counterstained with hematoxylin, and a negative control was performed following the same procedure without incubation with primary antibodies. Stained disks were visualized under light microscopy and imaged for analysis with the Q-Capture system.

Radiological evaluation

Postnatal growth of the spine was imaged using MRI (magnetic resonance imaging) in neonatal, 2-, and 6-week-old SD rats. Age-related IVDD was evaluated by X-ray radiography, CT (computed tomography) scanning, and MRI in mature (12 weeks old, 210–230 g) and aged (60 weeks old, 200–210 g) male SD rats. To avoid interference from breathing, rats were euthanized with CO_2; for the diameter limitation of the circular surface coil in CT scanning and MRI, the spine and paraspinal structures were harvested intact for imaging. X-ray radiography was performed with a Faxitron MX-20 X-ray machine at a voltage of 30 kV (Faxitron Bioptics, Wheeling, IL, USA). CT scans were acquired using a SkyScan 1176 radiograph microtomograph (Bruker microCT, Kontich, Belgium) with an exposure time of 340 ms and a rotation step of 0.9°, a voltage of 65 kv, and a current of 385 μA. MRI was performed using a BioSpec 7T/20 USR spect (Bruker BioSpin, Billerica, MA, USA; T2 TurboRARE, TE 25 ms, TR 2000 ms, thickness 0.7 mm).

Data acquisition and statistical analysis

On histological (HE) staining, all the vacuoles and nuclei on each evaluated section were identified and counted. The number of notochordal vacuoles was normalized to that of

the nuclei. The diameter of notochordal vacuoles was quantified by normalizing to the averaged nucleus diameter of 20 nuclei randomly selected out of each section. The areas of cartilaginous layers in the CEP and fibrotic portion in AF were measured and normalized to those of the CEP and AF, respectively, using ImageJ software (NIH, Bethesda, MD, USA). On immunohistochemical staining, staining for the target gene (Ki67 and PCNA) was counted in a minimum of 200 cells within the area of interest (NP, IAF, OAF, and CEP) and converted to a percentage to indicate expression intensity. Data were acquired from three consecutive mid-coronal sections covering the largest area of the NP and averaged to represent an analysis unit. In each group evaluated, a minimum of three rats were analyzed and results are presented as mean ± SD. Differences between groups were analyzed by one-way ANOVA followed by Tukey's multiple comparisons test. Within a specific group, differences between evaluated areas were analyzed by repeated–measures (RM) one-way ANOVA followed by Holm–Sidak's multiple comparisons test, using Prism software (ver. 6.0; GraphPad, San Diego, CA, USA). A P value < 0.05 was considered to indicate statistical significance.

Results

The NP, AF, and CEP of the IVD have different embryonic origins

To visualize the formation of the IVD, coronal sections of embryonic rat spine were evaluated by hematoxylin and eosin (HE) staining. At an early stage, at E13.5, anlagen of the prospective vertebrae and AF were evident as the paired and patterned sclerotome that contained a non-condensed cranial half and a condensed caudal half. Anlagen of the prospective NP, the axial notochord, were located between the paired sclerotomes (Fig. 1a). As development proceeded, the non-condensed sclerotome elongated axially and fused to form the vertebrae and CEP (Fig. 1b), whereas the condensed sclerotome expanded laterally to generate the AF, composed of a densely populated outer half and a non-densely populated inner half (Fig. 1c–d), with the inner AF and CEP being similar in cell density. Prior to E18.5, neither the forming IVD nor the vertebrae were vascularized; following the hypertrophic differentiation in the center of the cartilaginous vertebrae (Fig. 1c), primary ossification began and the newly formed disk became connected to the circulation system through the CEP (Fig. 1d). During the formation of vertebrae, the notochord (Fig. 1e) was segmented by the union of the paired vertebrae anlagen and compressed into the center of the prospective IVD, forming the NP, which was predominantly populated with vacuolated cells (Fig. 1f), some of which were retained within the CEP (Fig. 1g). From E14.5 to E18.5, the notochordal cells undergo significant dilatation of the cytoplasmic vacuoles (Fig. 1e–f). The NP of newborn IVD was populated exclusively by the vacuolated notochordal NP cells (Fig. 1h).

The inner AF and CEP share similar cellular and matrix components

To evaluate histocytological changes during disk formation, coronal sections of the embryonic spine were stained with Alcian blue (Fig. 2a–c) to assess the accumulation of cartilaginous matrix, with Picrosirius red staining (Fig. 2d–f) used for fibrotic matrix, Masson staining (Fig. 2g–i) used for collagenous fibers and myofibers, and PAS staining (Fig. 2j–l) used for glycoproteins and glycosaminoglycans. At E13.5–14.5, the pre-vertebrae non-condensed sclerotome accumulated both cartilaginous (Fig. 2a) and fibrotic matrix (Fig. 2d), in which PAS-positive glycoproteins and glycosaminoglycans were present (Fig. 2j–k) and more myofibers than collagenous fibers were observed (Fig. 2g–h). In contrast, except for myofibers (Fig. 2g), staining of the condensed sclerotome was negative for these chondrogenic differentiation-related matrix proteins (Fig. 2a, d, j). However, at E14.5–18.5, the extracellular matrix similar to those in the non-condensed sclerotome began to accumulate in the inner portion of the AF anlagen (Fig. 2h, k) and, by E18.5, no significant cellular or histological boundary existed between the inner AF and CEP (Fig. 2c, f, i, l). At E13.5–14.5, the notochord sheath also produced both cartilaginous (Fig. 2a) and fibrotic matrix (Fig. 2d) that might contain glycoproteins and glycosaminoglycans (Fig. 2j), and probably more collagenous fibers than myofibers (Fig. 2g). The notochord sheath was thick at E13.5, but became thinner and vanished (Fig. 2b, e) as the axial notochord was compressed into the prospective NP, in which more cartilaginous than fibrotic matrix accumulated (Fig. 2a–f).

The inner AF and CEP have similar potential of growth kinetics

Ki67 and PCNA are two commonly used markers of cell proliferation capacity. To investigate the growth kinetics among the different compartments within the developing IVD, expression of Ki67 and PCNA was evaluated by immunohistochemical staining in coronal sections of embryonic spine. At an early stage, at E13.5, non-condensed sclerotome, condensed sclerotome, and notochord showed approximately equal expression of Ki67 and PCNA (Figs. 3a, e, 4a). At E14.5, cell proliferation decreased in the outer portion of the condensed sclerotome and increased in the inner part of the AF anlagen, which showed similar expression of the proliferation markers to the pre-vertebrae non-condensed sclerotome (Figs. 3b, f, 4b). Similarly, at E18.5, the inner

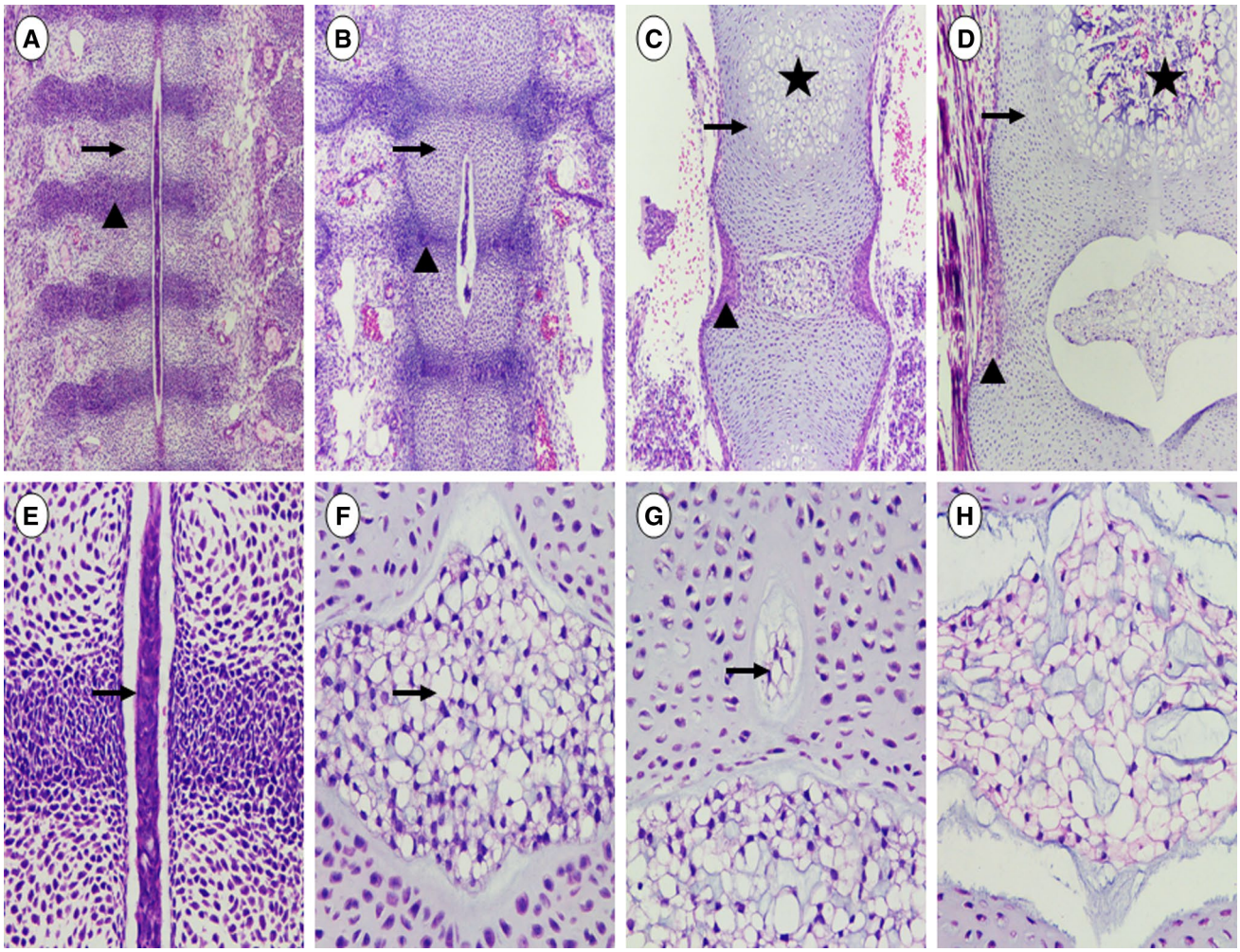

Fig. 1 HE staining of cellular changes during IVD formation. **a–d** Coronal sections of rat IVD at E13.5 (**a**), E14.5 (**b**), E18.5 (**c**), and neonatal (**d**). The condensed sclerotome (arrow head) generated the annulus fibrosus (AF), whereas the non-condensed sclerotome (arrow) developed into vertebrae and the cartilaginous endplate (CEP). Following hypertrophic changes (pentagram) within the cartilaginous vertebrae (**c**), a primary ossification center appeared (**d**). **e–f** Dilatation of cytoplasmic vacuoles during NP formation. At E13.5 (**e**), few vacuoles were detected within the notochord cells (arrow). By E18.5, the cytoplasmic vacuoles had increased significantly in both size and number (**f**). Some notochord cells were retained within the CEP (**g**), whereas the neonatal NP was populated exclusively with vacuolated cells (**h**). Original magnification ×100 for **a–d**, ×400 for **e–h**

AF and CEP showed equal expression of the proliferation markers that was higher than the outer AF (Figs. 3c, g, 4c), although the latter showed increased expression of Ki67 and PCNA postnatally (Figs. 3d, h, 4d).

Devacuolation of NP cells during maturation and aging

To visualize the cellular changes during IVD maturation and aging, coronal sections of postnatal rat disk were assessed with HE staining (Fig. 5a–d; Fig. 6a–b). In contrast to the inflation of the notochordal vacuoles during NP formation (Fig. 1e–f), the cytoplasmic vacuoles decreased significantly in both size and number from 4 to 60 weeks old (Fig. 5a–d). However, when normalized to nuclei, the number of notochordal vacuoles increased postnatally until 4 weeks of age (Fig. 5e–f). In the aged IVD of 60-week-old rat, both large acellular zones and cell clusters were detected within the NP (Fig. 6a–b). As shown by a series of histological sections of IVD (Fig. 7), the adult (12–30 weeks old) NP showed primarily accumulated cartilaginous matrix (Fig. 7h–i) that was positive for glycoproteins and glycosaminoglycans (Fig. 7r–s), but stained less for collagenous fibers (Fig. 7m–n). However, in the acellular zones of the aged NP of 60-week-old rat, staining for cartilaginous matrix decreased, while that for collagenous fibers increased (Fig. 7j, o, t).

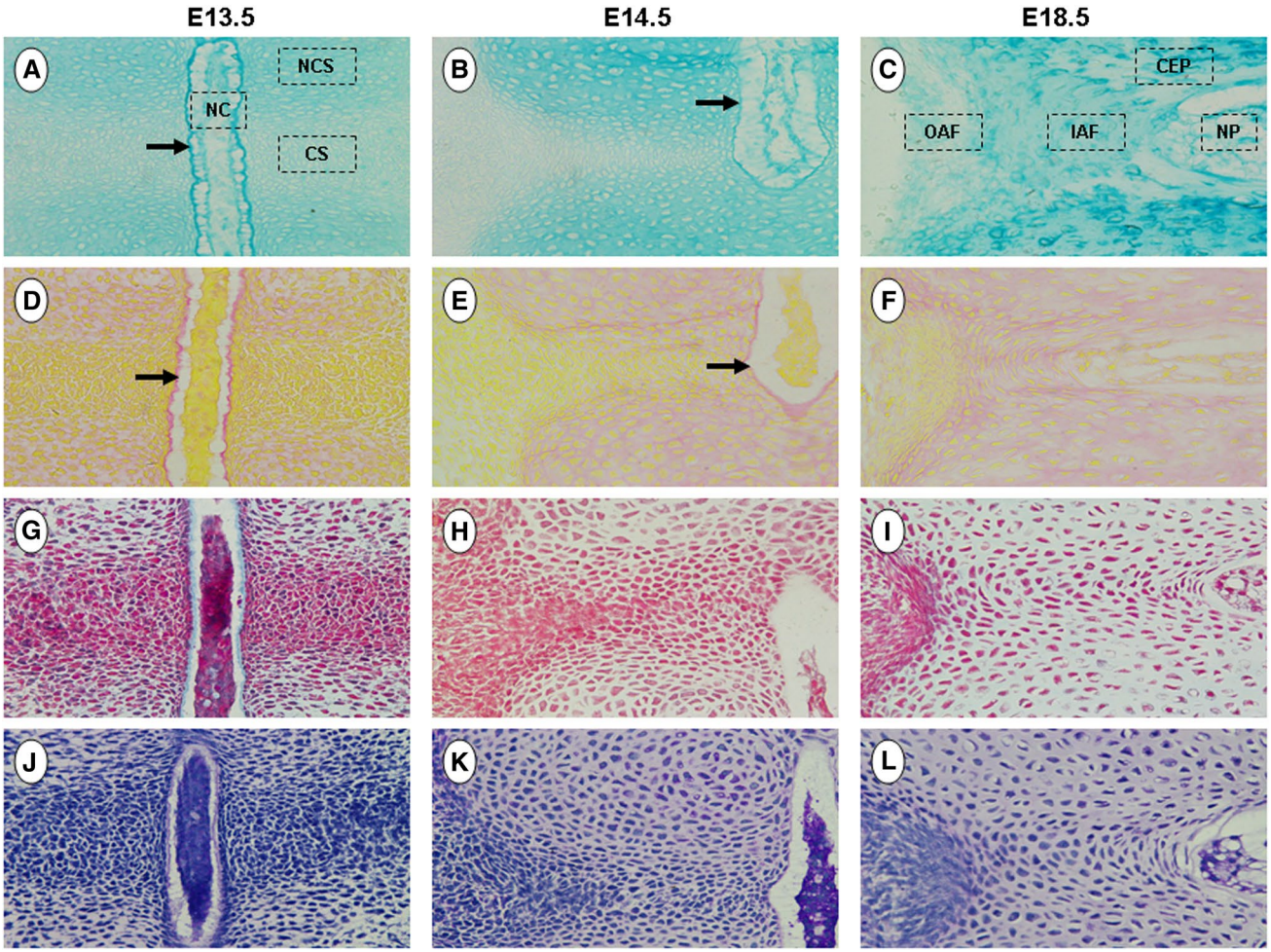

Fig. 2 Staining of histological changes during IVD formation. **a–c** Alcian blue staining. At E13.5, the non-condensed sclerotome, notochord, and notochord sheath (arrow) were stained light blue, whereas the condensed sclerotome was negative for cartilaginous matrix staining. At E14.5–18.5, the notochord sheath became thinner and disappeared while the blue-stained cartilaginous matrix began to accumulate in the inner AF. **d–f**. Picrosirius red staining. Except for the notochord, the red-stained fibrotic matrix accumulated initially in non-condensed sclerotome and notochord sheath (arrow) at E13.5–14.5 and later in the inner AF at E18.5. **g–i**. Masson staining. At E13.5, the notochord sheath stained blue for collagenous fibers, whereas more red-stained myofibers accumulated in the condensed sclerotome and notochord than in the non-condensed sclerotome. At E14.5–18.5, the inner AF and CEP began to show similar fiber contents, while the myofibers within the notochord decreased, compared with E13.5. **j–l** PAS staining. PAS-positive matrix was stained light red and detected primarily in the axial notochord and notochord sheath at E13.5 and accumulated in the non-condensed sclerotome at E14.5–18.5. Again, the CEP and inner AF showed a similarly PAS-positive matrix. *NC* notochord, *CS* condensed sclerotome, *NCS* non-condensed sclerotome, *NP* nucleus pulposus, *IAF* inner annulus fibrosus, *OAF* outer annulus fibrosus, *CEP* cartilaginous endplate. Original magnification ×400

Narrowing of cartilaginous layers of the endplate during maturation and aging

On histological sections of the postnatal rat IVD (Fig. 7), CEP also showed significant age-related histocytological changes. First, the thick cartilaginous layers of the neonatal endplate became thinner as growth plate elongated and vertebrae grew (Fig. 7a–c); during this process, the cartilaginous matrix decreased, whereas the fibrotic matrix increased within the CEP (Fig. 7f–h), which was rich in collagenous fibers (Fig. 7k–m) and PAS-positive glycoproteins and glycosaminoglycans (Fig. 7p–r). Second, after secondary ossification began (Fig. 8a, b), from the peripheral region of the CEP and then infiltrating outward, the cartilaginous layers of the endplate significantly narrowed (Figs. 7d, e, 8c); during this process, myofibers increased while collagenous fibers and PAS-positive components decreased (Fig. 7i, j, n, o, s, t).

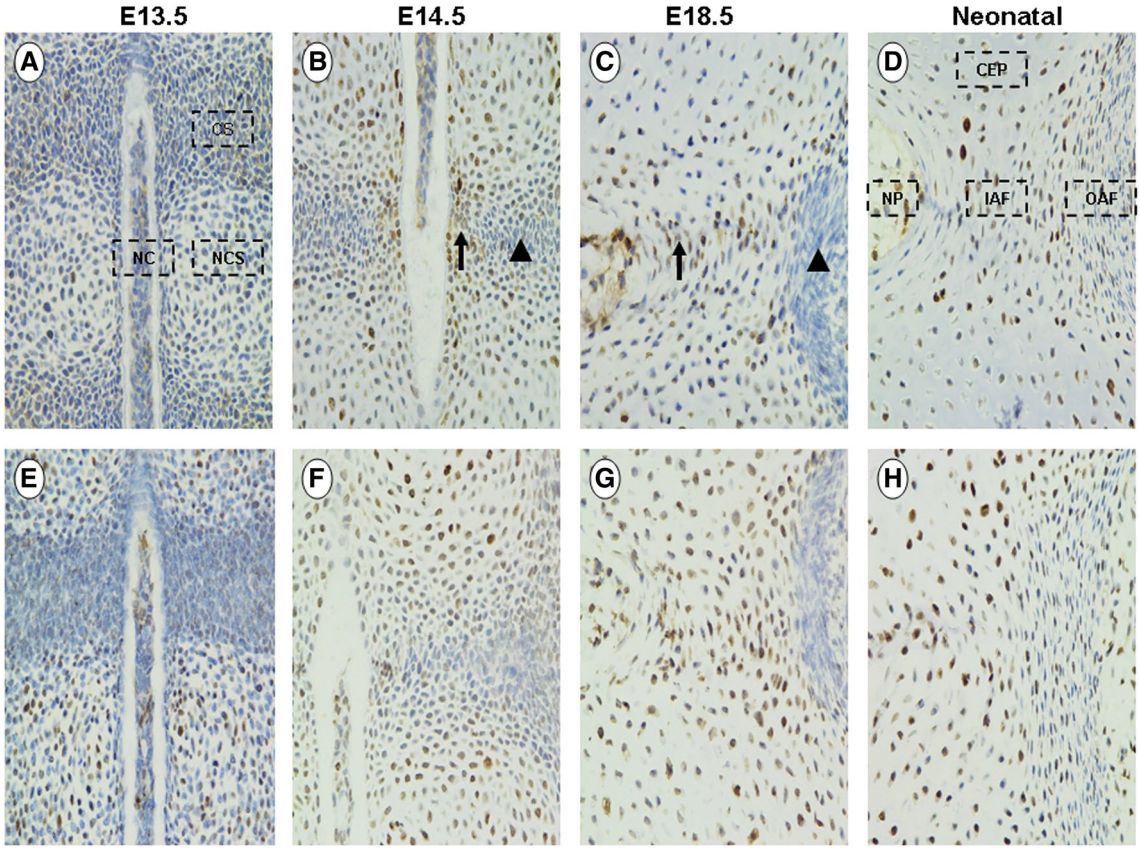

Fig. 3 Immunohistochemical staining of Ki67 and proliferating cell nuclear antigen (PCNA) during IVD formation. **a–d**. Immunohistochemical staining for Ki67 in embryonic and neonatal rat IVD. At E13.5, Ki67 showed equivalent levels in the non-condensed sclerotome, condensed sclerotome, and notochord. At E14.5, Ki67 was expressed less in the outer portion of the condensed sclerotome (arrow head) than in the inner part (arrow), which showed a similar expression pattern of Ki67 as the pre-vertebrae non-condensed sclerotome. At E18.5, the outer AF (arrow head) showed even less Ki67 than the inner AF (arrow), which showed no significant difference in the expression of Ki67 versus the NP and CEP. In the neonatal IVD, the inner AF and CEP were still similar in the expression of Ki67, which was higher than that of the outer AF, although the latter showed increased positivity of Ki67 staining as compared with E18.5. **e–h** Immunohistochemical staining for PCNA. PCNA was expressed and localized in a pattern similar to that of Ki67 in embryonic and neonatal rat IVD. *NC* notochord, *CS* condensed sclerotome, *NCS* non-condensed sclerotome, *ICS* inner portion of the condensed sclerotome, *OCS* outer portion of the condensed sclerotome, *NP* nucleus pulposus, *IAF* inner annulus fibrosus, *OAF* outer annulus fibrosus, *CEP* cartilaginous endplate. Negative controls are not shown. Original magnification ×400

Narrowing of the fibrotic portion of the AF during maturation and aging

As shown by histological staining, distinct histocytological boundaries separated the inner and outer AF of the neonatal IVD, where the inner AF was cartilaginous while the outer AF showed accumulated fibrotic matrix (Fig. 9a, f). With maturation, the histocytological boundaries became increasingly indistinct and the inner cartilaginous matrix began to accumulate within the outer fibrotic AF (Fig. 9b–d, g–i), reducing the ratio of the fibrotic layers to the entire AF (Fig. 8d). In the aged AF of 60-week-old rat, large longitudinal fissures were detected near the transitional area between the inner and outer AF (Fig. 9e), where cartilaginous matrix also accumulated (Fig. 9j). Unlike the cartilaginous matrix of the NP, the AF was stained more positively for collagenous fibers (Fig. 9k–m) and, as aging progressed, myofibers increased regionally within the cartilaginous matrix of the aged AF of 60-week-old rat (Fig. 9o), which became less positive for Alcian blue and PAS staining (Fig. 9j, t).

Radiological evidence of disk growth, maturation, and age-related degeneration

To investigate postnatal growth of the IVD, MRI (magnetic resonance imaging) was performed on neonatal, 2-, and 6-week-old rat spines. In the neonatal rat, the NP of the lower thoracic region was not as fully hydrated as the lumbar NP (Fig. 10a), which took an additional 2 weeks to demonstrate a bright disk on T2-weighted images (Fig. 10b, c). To visualize age-related IVDD by radiology, X-ray radiography,

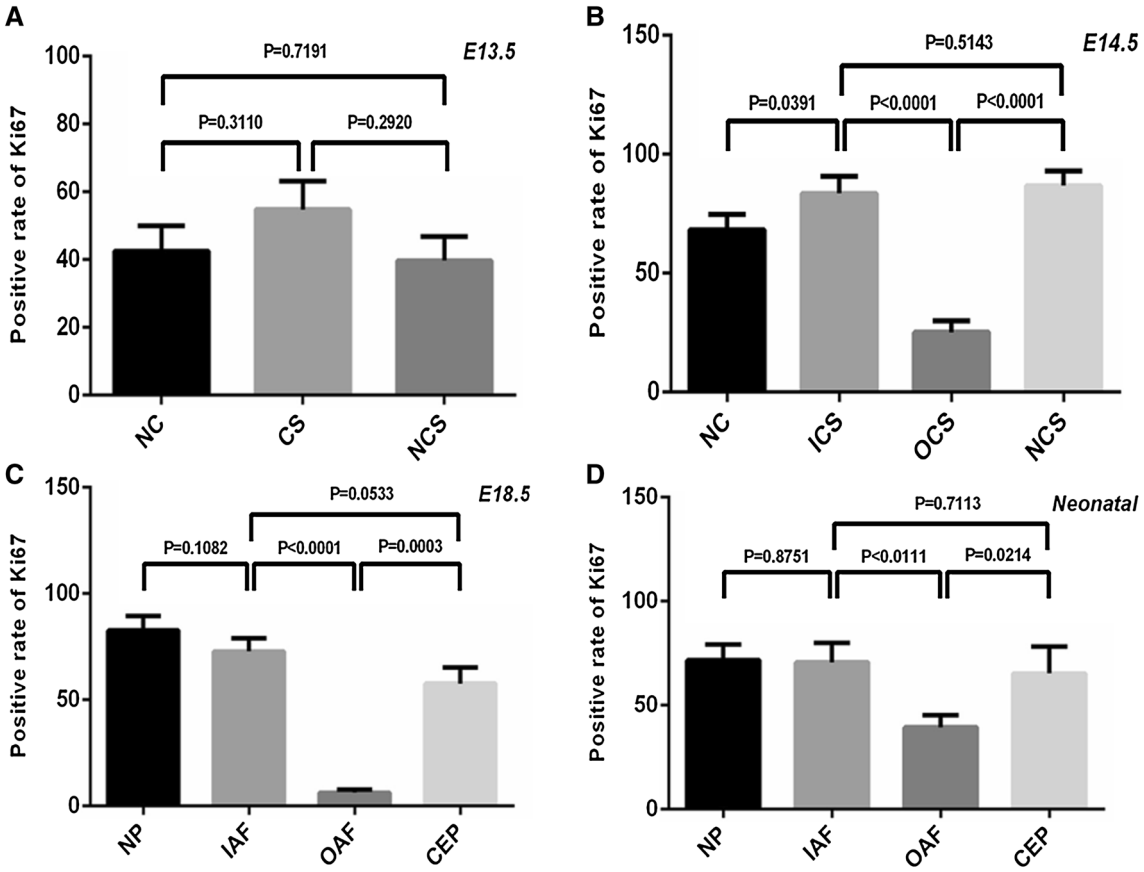

Fig. 4 Statistics of immunopositivity for Ki67 expression during IVD formation. *NC* notochord, *CS* condensed sclerotome, *NCS* non-condensed sclerotome, *ICS* inner portion of the condensed sclerotome, *OCS* outer portion of the condensed sclerotome, *NP* nucleus pulposus, *IAF* inner annulus fibrosus, *OAF* outer annulus fibrosus, *CEP* cartilaginous endplate. Statistics for the expression of PCNA are not shown

computed tomography (CT) scanning, and MRI were performed on 12- and 60-week-old rat spines. As aging progressed, the growth plate of younger rats, which was radioparent on X-ray radiography and CT scanning (Fig. 10d–g), vanished gradually and, with secondary ossification, fused with the vertebrae (Fig. 10i–l). On MRI, the T2 signals of younger IVD were bright and compartmentalized mainly within the NP and/or inner AF (Fig. 10h), whereas the aged and dehydrated disk of 60-week-old rat grossly lost T2 signals and the radiological boundaries between NP and AF became less distinct (Fig. 10m).

Discussion

The theoretical basis for the study described here was that some IVDs are probably dysgenerated during embryogenesis and are never well developed, and yet appear as normal on radiology scans [8, 13, 14]. Through a series of histocytological observations in embryonic rat spine, we showed that constructing a well-structured and fully hydrated disk appears to require, at least: (1) unification of the paired non-condensed sclerotome that segments and compresses the axial notochord into the NP, (2) dilatation of notochordal cytoplasmic vacuoles to generate vacuolated NP cells, and (3) restrained growth kinetics in the outer condensed sclerotome that might facilitate or synchronize the expansion of the inner AF and NP. Because constructing the IVD is a multifaceted and orchestrated process, any impairment of the critical developmental steps could possibly lead to a dysgenerated IVD. For example, failed fusion of the paired pre-vertebrae sclerotome might generate inherent lesions in the CEP that potentiate the intravertebral herniation of the NP [25] or cause Schmorl's node [26, 27]; also, defects in the dilatation of notochordal vacuoles could possibly lead to a narrowed disk with reduced T2 signal intensity, as reported in adolescent spines [12]. Our results are consistent with these notions, showing that the newly formed NP could be arrested within the CEP, which, in turn, may diminish the notochord content in the prospective IVD. This is also consistent with the prevalence of chordomas in the spheno-occipital and sacrococcygeal regions, where the IVD

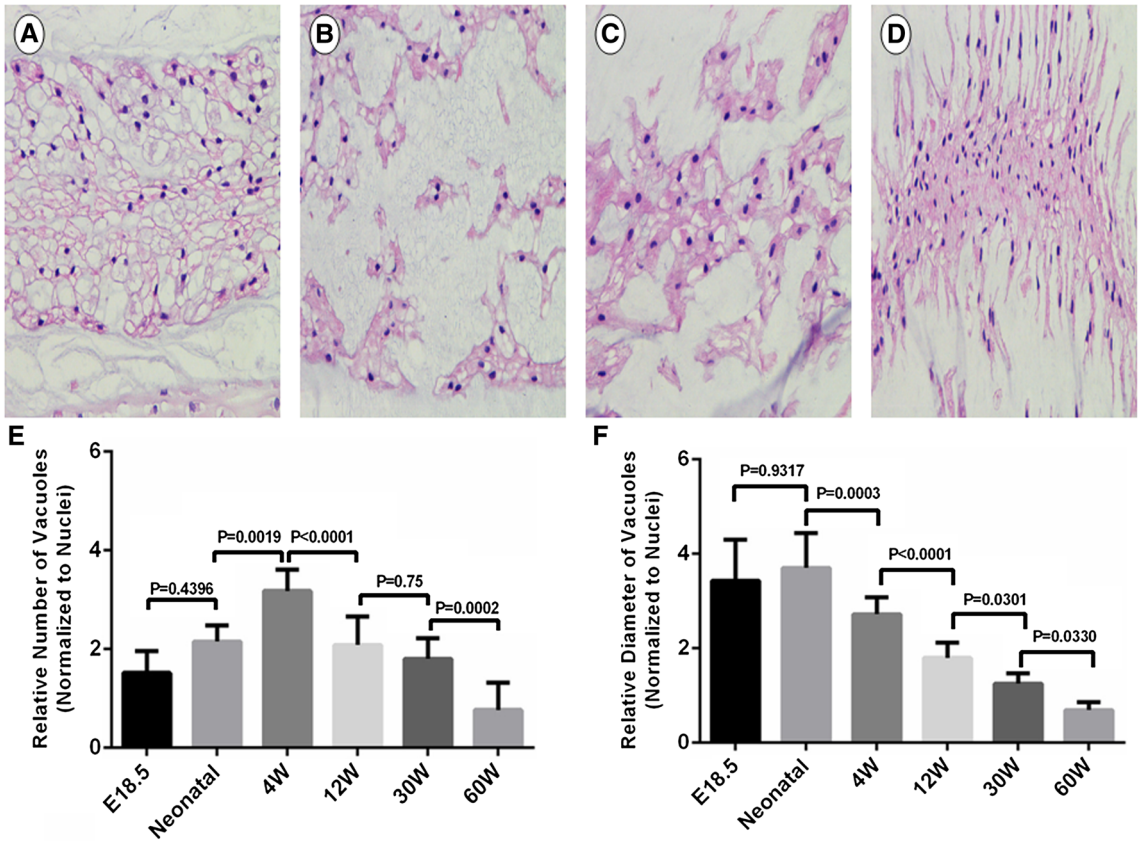

Fig. 5 HE staining of NP during IVD degeneration. **a**–**d** Vanishing of cytoplasmic vacuoles during aging and degeneration. The vacuoles decreased significantly in both size and number from 4 weeks (**a**) to 12 weeks (**b**), 30 weeks (**c**), and 60 weeks old (**d**). **e**–**f** Statistics of the notochordal vacuoles during IVD formation and degeneration. While the diameters of vacuoles showed steady reductions as aging progressed (**f**), the number of cytoplasmic vacuoles increased until 4 weeks old and then decreased (**e**). Original magnification ×400 for **a**–**d**

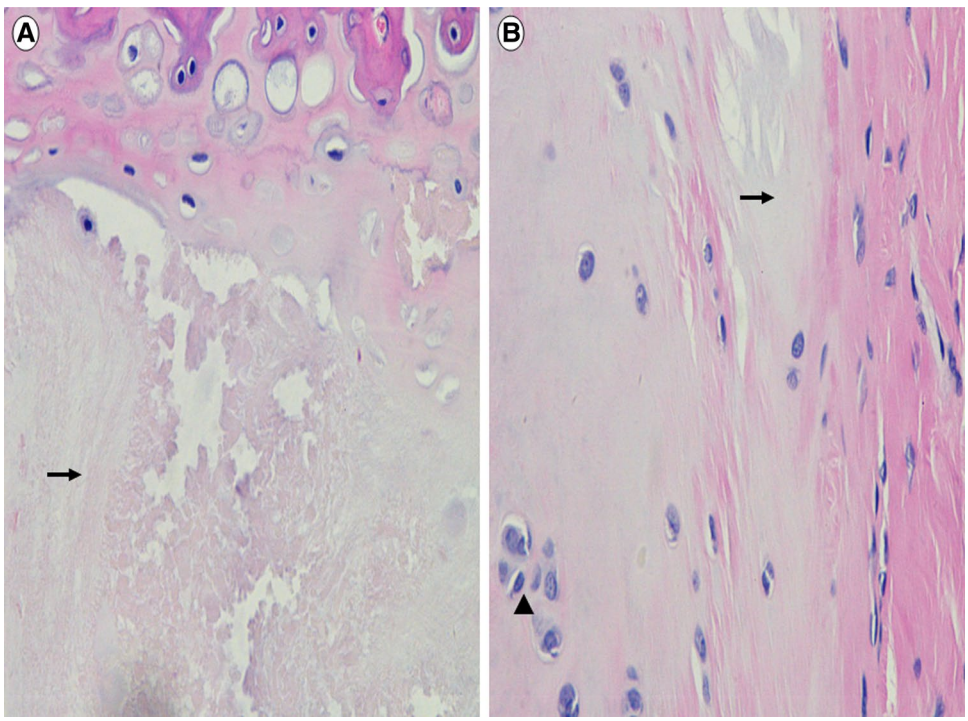

Fig. 6 HE staining of acellular zones and cell clusters in degenerated NP. Within the NP of degenerated disk (60 weeks old), large acellular zones (arrow) and cell clusters (or regionally proliferation-enhanced zones, arrow head) were evident. Original magnification ×400 for **a**, **b**

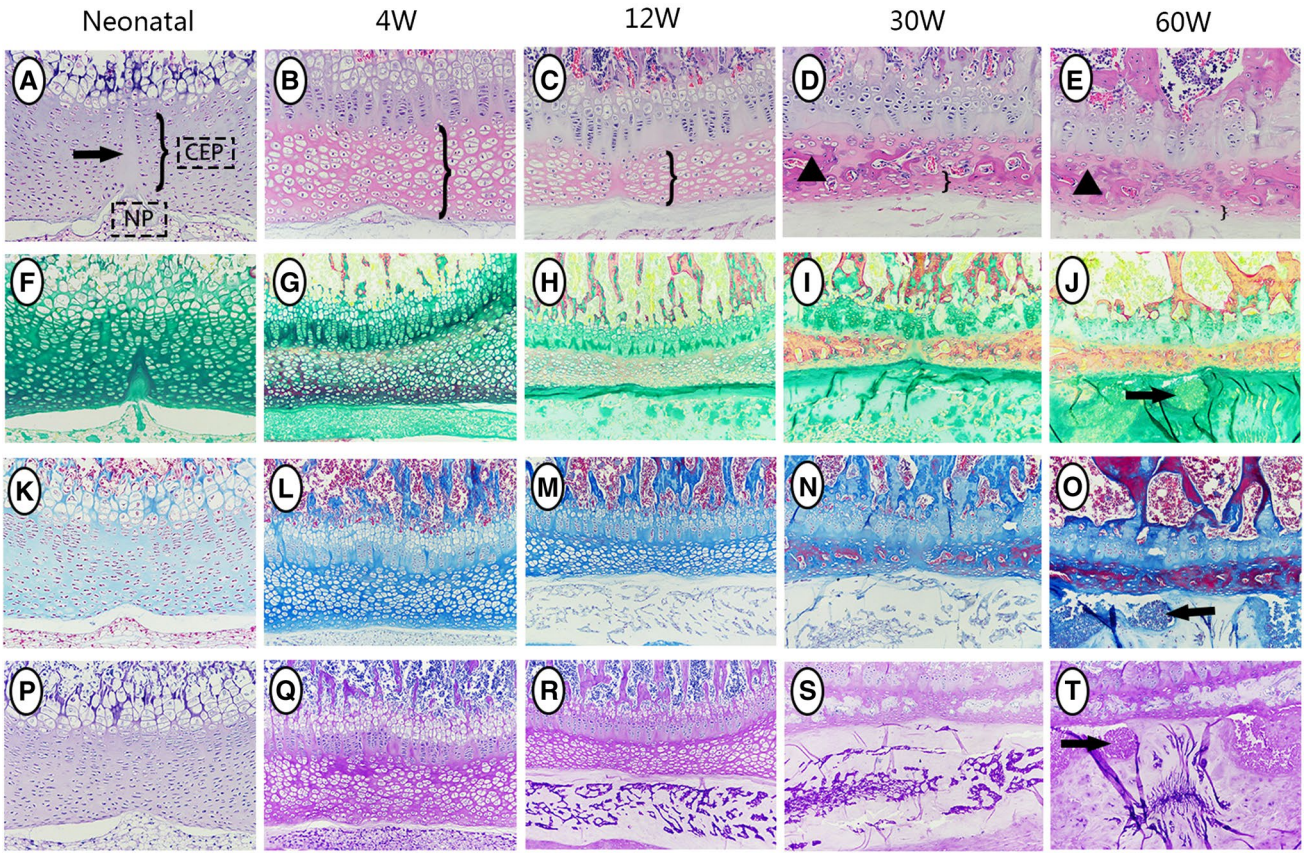

Fig. 7 Histological staining of the postnatal change within CEP and NP. **a**–**e** HE staining. In the neonatal endplate, the cartilaginous layers were thick (bracket) and the fusion line between the paired vertebrae anlagen was visible (arrow). At 4–12 weeks, the cartilaginous layers became comparatively thinner as the growth plate extended toward the endplate surface. At 30–60 weeks, secondary ossification (arrow head) narrowed the cartilaginous layers significantly, although activity of the growth plate ceased. **f**–**j** Alcian blue and Picrosirius red staining. In the neonatal endplate, the green-stained cartilaginous matrix accumulated predominately. At 4–12 weeks, cartilaginous matrix decreased while the red-stained fibrotic matrix increased within the CEP. At 30–60 weeks, secondary ossification resulted in more fibrotic matrix. **k**–**o** Masson staining. In the neonatal endplate, blue-stained collagenous fibers accumulated initially. At 4–12 weeks, collagenous fibers increased significantly within the cartilaginous layers, which were replaced later (30–60 weeks old) by the red-stained myofibers as secondary ossification progressed. **p**–**t** PAS staining. The PAS-positive matrix was stained light red and accumulated in the cartilaginous layers of the younger endplate (neonatal to 12 weeks old), which also decreased after secondary ossification began. The NP of the adult (12–30 weeks old) rat accumulated primarily cartilaginous matrix (**h**–**i**) that was positive for glycoproteins and glycosaminoglycans (**r**–**s**), but stained less for collagenous fibers (**m**–**n**). In contrast, the large acellular zones within the degenerated NP (arrow) stained less with Alcian blue (**j**) but were positive for collagenous fibers (**o**) and PAS staining (**t**). *NP* nucleus pulposus, *CEP* cartilaginous endplate original magnification ×200

is morphologically atrophied or missing [28]. Moreover, the postnatal swelling of the lower thoracic NP and increase in cytoplasmic vacuoles until the ages of 4 weeks support the need for notochord expansion and hydration to manifest the plump and bright disk on MRI. This is in accordance with the finding that the narrowed dysgenerated IVDs are more prevalent in the upper lumbar and thoracic segments than in the lower spine in adolescents [12, 25].

Evidence is mounting that the axial notochord provides both mechanical and signal support for the development of the vertebral column [15, 16]. To date, the notochord has been known to release numerous signaling factors, such as sonic hedgehog (SHH) and noggin, to regulate the patterning and differentiation of presomitic paraxial mesoderm [29–31], and undergo fast vacuolation to elongate and maintain the geometry shape of forming spine [32]. Recent studies in *Xenopus laevis* revealed that the matrix (fibronectin and laminin) deposited at notochord–somite boundaries functioned through specific transmembrane receptors, such as integrin and dystroglycan, to potentiate polarization of the paraxial mesoderm and vacuolation of the axial notochord [33]. We noticed that although the thick notochord sheath of rat embryos accumulated both cartilaginous and fibrotic matrix—rich in collagenous fibers, glycoproteins, and glycosaminoglycans—it thinned gradually and vanished as the unvacuolated notochord became compressed into the

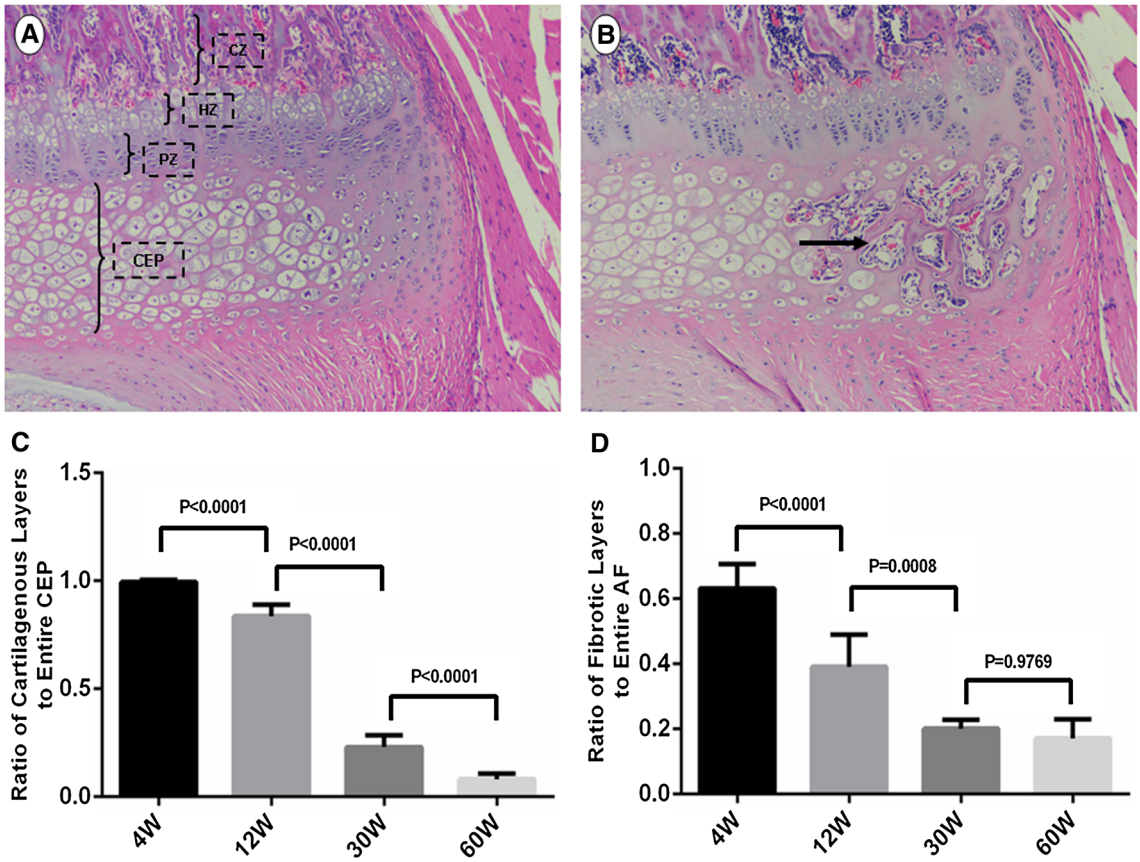

Fig. 8 HE staining of secondary ossification during IVD maturation. **a**, **b** HE staining of rat vertebral endplate at 4 weeks (**a**) and 12 weeks (**b**) old. The vertebral endplate was resulted from endochondral ossification, located at the cranial and caudal end of the vertebrae, mainly composed of chondrocytes separating nucleus pulposus from bone marrow cavity. Like the cartilaginous end in long bones, and based on the maturity of chondrocytes, the vertebral endplate could also be divided into (1) zone of resting chondrocytes, which was located adjacent to the nucleus pulposus, (2) zone of proliferating chondrocytes, also known as growth plate, (3) zone of hypertrophic chondrocytes, and (4) zone of apoptosis and calcification (ossification center), which featured vascularization and was connected to the circulation system. The cartilaginous endplate (CEP) usually refers to the resting chondrocyte layers that connect IVD to the growth plate of vertebrae. During maturation, secondary ossification (arrow) initiated from the peripheral region of CEP and then infiltrated inward, reducing the cartilaginous layers therein. **c**, **d** Statistics of postnatal changes within rat CEP and AF. Both the cartilaginous layers in CEP and the proportion of fibrotic AF showed steady reductions during IVD maturation and aging. *CEP* cartilaginous endplate, *PZ* proliferating zone, *HZ* hypertrophic zone, *CZ* calcification zone. Original magnification ×400 for **a**, **b**

prospective IVD. Choi et al. [29] found that SHH signaling mediated the formation of the notochord sheath and that the latter was responsible for moving notochord cells into the forming disks. Because the notochord sheath will disassemble as the IVD forms, it is possible that some notochord cells may leak out through the broken sheath and be retained within the vertebrae or CEP. However, by far, it remains largely unclear why the notochord sheath disappears during formation of the NP, and whether disassembly of the sheath is related to the vacuolation process that follows within the mammalian notochord. Based on the insufficient vacuolation before E14.5 and the vanishing of notochord sheath afterward, we suggest that vacuole-derived hydrostatic pressure may provide little, or no, mechanical support for vertebrate body elongation in rat embryos. Instead, unlike zebrafish [32, 34, 35], axial growth of the embryonic rat spine may rely more on chondrogenic differentiation and elongation of the non-condensed sclerotome, supporting the notion that the vertebral column is generated in an evolution-dependent and species-specific manner [15, 16, 21–24].

Regarding the long-debated issue of cellular heterogeneity within the IVD [17–20], we showed clearly that: (1) the NP was derived from the axial notochord and was populated exclusively with vacuolated cells, supporting the view that all NP cells, including the non-vacuolated chondrocytes in the adult NP may be of notochord origin [19, 20], (2) the CEP developed from non-condensed sclerotome but contained mixed notochord cells, so was heterogeneous, and (3) the AF originated from the condensed sclerotome, although its inner part was histocytologically

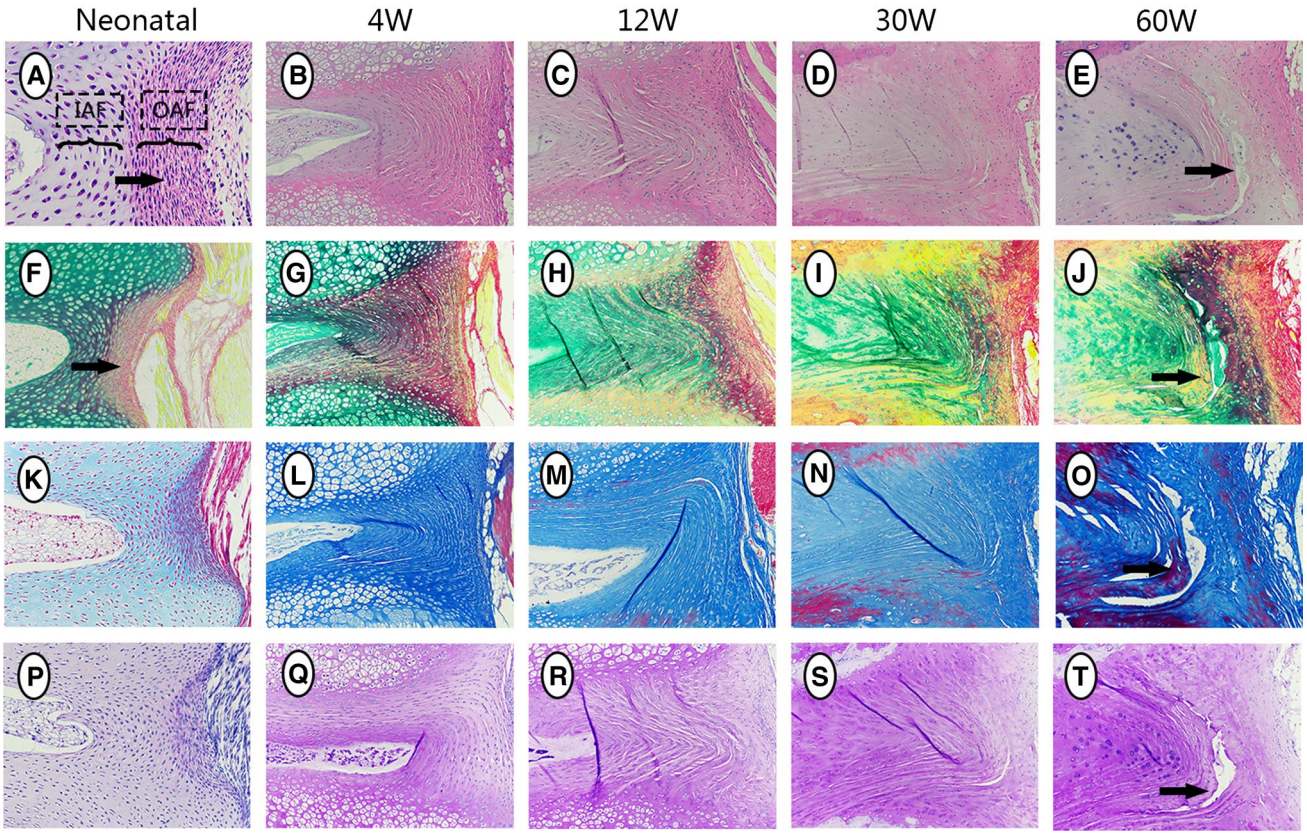

Fig. 9 Histological staining of postnatal changes within the AF. **a–e** HE staining. In the neonatal IVD (**a**), distinct boundaries separated the NP, inner AF, and outer AF from each other, with the latter being much more densely populated (arrow). As aging progressed (4–30 weeks old), the anatomical boundaries became less distinct, especially between the inner and the outer AF, where the cell densities were similar. **f–j**. Alcian blue and Picrosirius red staining. In the neonatal AF (**f**), the inner part accumulated green-stained cartilaginous matrix while the outer part showed red-stained fibrotic matrix (arrow). During aging, the inner cartilaginous matrix gradually infiltrated outward and decreased the fibrotic portion of the AF. **k–o** Masson staining. Both the blue-stained collagenous fibers and the red-stained myofibers were detected in the neonatal AF (**k**), whereas as the rat matured and aged, collagenous fibers accumulated predominately within the AF. **p–t** PAS staining. PAS-positive matrix was detected in both the inner and outer portions of neonatal AF, which accumulated mainly within the inner AF as aging progressed. In the aged AF of 60-week-old rat (**e**), large longitudinal fissures were evident (arrow) and the matrix therein was positive for Alcian blue (**j**) but negative for collagenous fibers (**o**) and PAS staining (**t**); regionally, Alcian blue (**j**) and PAS staining (**t**) was decreased while myofibers (**o**) increased within the cartilaginous AF of 60-week-old rat (arrow). *IAF* inner annulus fibrosus, *OAF* outer annulus fibrosus. Original magnification ×200

similar to the adjacent CEP, raising the possibility that the AF might originate heterogeneously from both the condensed sclerotome and pre-vertebrae non-condensed sclerotome. Making this issue even more complex, the resegmentation theory [24] states that the non-condensed sclerotome generates only the lower CEP of a single vertebra, whereas the upper CEP is constructed from part of the condensed sclerotome from a cranial somite. However, probably because of the differentiation-based histological analyses, the resegmentation process of the rat vertebral column was not detected in our study. Also, our findings are inconsistent with an early report that the caudal condensed half of the chick sclerotome demonstrated higher proliferation than the cranial non-condensed halves [36]. Further observations across species and cell lineage studies are required to unveil the full embryonic origin of all the components of the IVD.

Of the increasing list of factors that lead to IVDD, natural aging is supposed to cause the most substantial and irreversible degenerative changes [3]. Here, we showed that as aging progressed, the vacuolated notochord NP cells were gradually exhausted and replaced by chondrocytic NP cells; the cartilaginous layers of CEP were narrowed as the vertebrae grew and secondary ossification began, and the cartilaginous matrix of the inner AF infiltrated outward and reduced the thickness of the fibrotic AF. These age-related degenerative changes take longer time to be than the degeneration induced by annulus puncture or mechanical overloading, which often features acute loss of NP content and collapsed IVD [37, 38]. Previously, the notochordal NP cells were considered

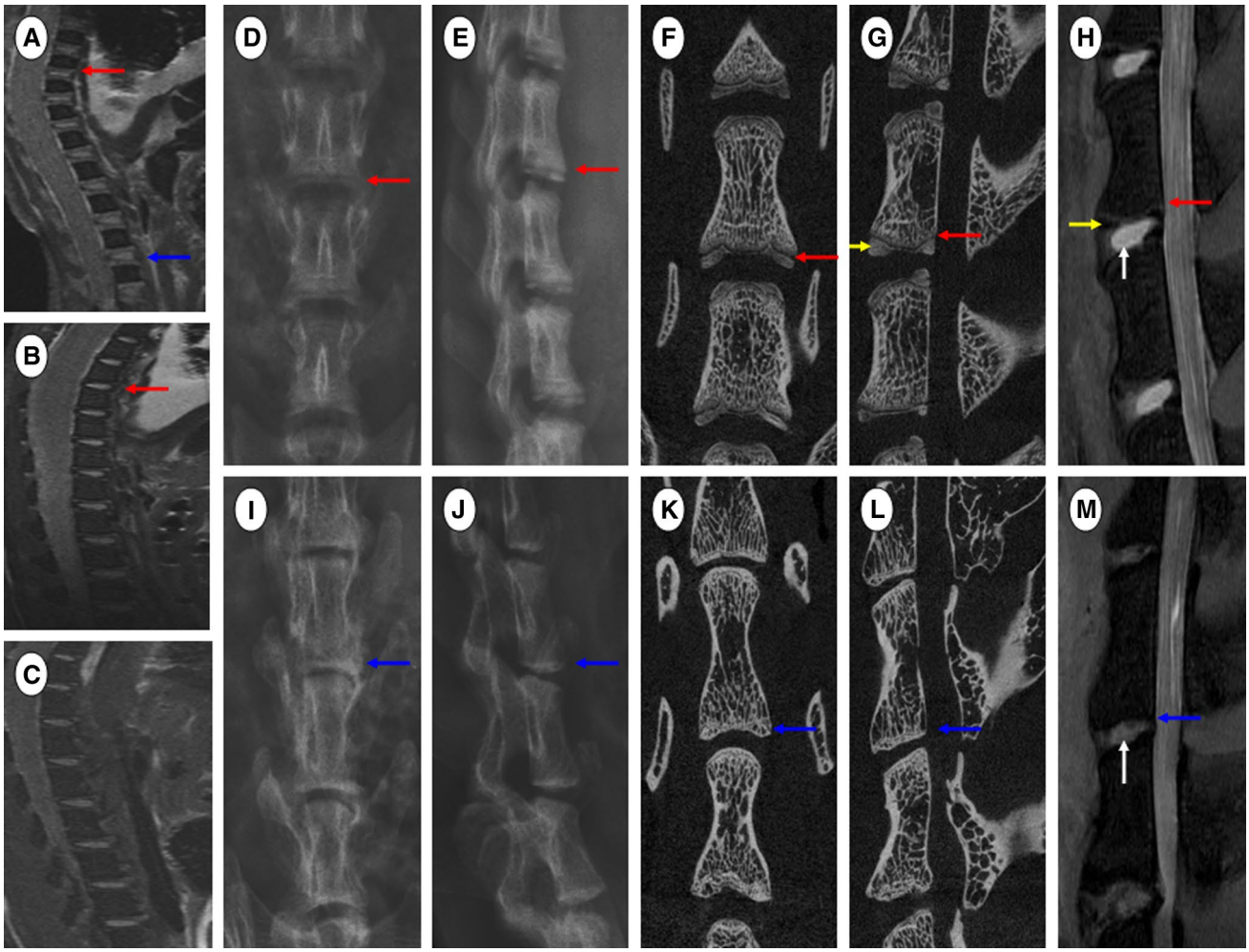

Fig. 10 Radiological evaluation of postnatal growth and age-related degeneration in the rat IVD. **a**–**c** Magnetic resonance imaging (MRI) scans of neonatal (**a**), 2- (**b**), and 6-week-old (**c**) rat spines. In the neonatal IVD, the lumbar NP (blue arrow) was expanded and hydrated to a higher extent than the lower thoracic NP (red arrow), which took an additional 2 weeks to show a T2-weighted signal (B, red arrow). **d**–**m**. X-ray radiography (**d**–**e**, **i**–**j**), computed tomography (CT) scan (**f**–**g**, **k**–**l**), and MRI (**h**, **m**) scan of 12-week- (**d**–**h**) and 60-week-old (**i**–**m**) rat spine. At 12 weeks, the growth plate of the vertebrae was visible as a radioparent epiphysis line (red arrow) on X-ray radiography (**d**–**e**) and CT (**f**–**g**) scanning, while on MRI, it demonstrated a high T2-weighted signal that was bright (**h**), and vanished in the aged spine (blue arrow). At 12 weeks old, the secondary ossification that initiated from the peripheral region of the CEP showed high intensity signals on CT scanning (**g**, yellow arrow) but low T2 signals on MRI (**h**, yellow arrow), which infiltrated inward and fused with the vertebrae in the aged spine. In the younger IVD, the T2 signals were bright and compartmentalized primarily within the NP and/or inner AF (**h**, white arrow), whereas an aged and dehydrated disk grossly lost T2 signals and the radiological boundaries between the NP and AF became indistinct (**m**, white arrow)

to become self-exhausted due to Fas-mediated apoptosis, and to be replaced by chondrocytes migrating from the CEP [39–41]. However, we found just the opposite to the vacuolation process during NP formation, the aging NP showed devacuolation and the cytoplasmic vacuoles were reduced in both size and number, suggesting that a chronic transition into chondrocytic NP cells, probably in addition to acute cellular apoptosis [39], may account for the age-related exhaustion of the vacuolated notochord cell resources. Noteworthy, most of human notochordal NP cells have transformed into chondrocyte-like NP cells before skeletal maturity, and early onset of IVDD is common in adolescents [42]. Similar IVD degeneration pattern also exists in the chondrodystrophic dog [43], suggesting that age-related IVD degeneration could be initiated and promoted in a species-specific manner. Further observations across species are also required to characterize the age-related degenerative change in mammal IVD.

For IVD regeneration, therapies ranging from growth factor injection to stem cell transplantation have been tested in a variety of IVDD models [2, 42, 43]. Because a degenerated disk, as seen in the aged rat of 60 weeks old, featured gross

degeneration in the NP, AF, and CEP, caution should be taken when judging that the disk is "regenerated" after the NP, presumably the most important structure of the three, is supplemented with therapeutic ingredients [2, 44]. More importantly, as T2-weighted MR imaging shows mainly the overall content of the hydrated matrix [10, 45, 46], a bright disk does not necessarily mean a healthy or regenerated one, given that the outward infiltration of cartilaginous matrix is degenerative and the cellular components within may have changed. Similar concerns also apply to association studies, where the "degenerative" group, assigned according to radiology results, may be highly heterogeneous in terms of the molecular basis, histopathological cascades, and genetic dispositions that lead to the IVD with reduced signal intensity; thus, there is a need to revamp the classification scheme for IVDD [8]. Recently, accumulating evidence has suggested that the avascular IVD itself may have already inherited stem cells or attracted progenitors from specific stem cell niches for endogenous repairs [2, 47–49]. Considering the natural history of IVD, from embryonic formation to age-related degeneration, it is perhaps not surprising that these inherent multipotent cells are diversified in terms of both identity and functionality [2, 49]. Because these resident disk stem cells are incapable of halting age-related IVDD, it remains debatable as to whether transplanted stem cells are capable of providing an efficacious and durable therapeutic effect [2]. To achieve long-term promising regeneration, age-related IVDD should be targeted and alleviated in the first place, before we encourage the clinical practice of any biological disk repairs.

Acknowledgement This study was supported by the National Natural Science Foundation of China (No. 81201423, No. 81272035, No. 81572170) and the Fundamental Research Funds of the Central Universities (No. 2242017K3DN06). The authors would like to acknowledge He-Ling Fu, Yuan Zheng, and Dan Bao, from the Animal Core facility of Nanjing Medical University, for their aids in radiological imaging and analysis.

Compliance with ethical standards

Conflict of interest None.

References

1. Risbud MV, Shapiro IM (2014) Role of cytokines in intervertebral disc degeneration: pain and disc content. Nat Rev Rheumatol 10(1):44–56
2. Wang F, Shi R, Cai F, Wang YT, Wu XT (2015) Stem cell approaches to intervertebral disc regeneration: obstacles from the disc microenvironment. Stem Cells Dev 24(21):2479–2495
3. Wang F, Cai F, Shi R, Wang XH, Wu XT (2016) Aging and age related stresses: a senescence mechanism of intervertebral disc degeneration. Osteoarthritis Cartilage 24(3):398–408
4. Vos T, Flaxman AD, Naghavi M, Lozano R et al (2012) Years lived with disability (YLDs) for 1160 sequelae of 289 diseases and injuries 1990–2010: a systematic analysis for the Global Burden of Disease Study 2010. Lancet 380(9859):2163–2196
5. Wu X, Zhuang S, Mao Z, Chen H (2006) Microendoscopic discectomy for lumbar disc herniation: surgical technique and outcome in 873 consecutive cases. Spine 31(23):2689–2694
6. Sinkemani A, Hong X, Gao ZX, Zhuang SY et al (2015) Outcomes of microendoscopic discectomy and percutaneous transforaminal endoscopic discectomy for the treatment of lumbar disc herniation: a comparative retrospective study. Asian Spine J 9(6):833–840
7. Wang K, Hong X, Zhou BY, Bao JP et al (2015) Evaluation of transforaminal endoscopic lumbar discectomy in the treatment of lumbar disc herniation. Int Orthop 39(8):1599–1604
8. Luk KD, Samartzis D (2015) Intervertebral disc "dysgeneration". Spine J 15(9):1915–1918
9. Pfirrmann CW, Metzdorf A, Zanetti M, Hodler J, Boos N (2001) Magnetic resonance classification of lumbar intervertebral disc degeneration. Spine 26(17):1873–1878
10. Davies BM, Atkinson RA, Ludwinski F, Freemont AJ et al (2016) Qualitative grading of disc degeneration by magnetic resonance in the lumbar and cervical spine: lack of correlation with histology in surgical cases. Br J Neurosurg 30(4):414–421
11. Battie MC, Videman T, Levalahti E, Gill K, Kaprio J (2007) Heritability of low back pain and the role of disc degeneration. Pain 131(3):272–280
12. Samartzis D, Karppinen J, Mok F, Fong DY, Luk KD, Cheung KM (2011) A population-based study of juvenile disc degeneration and its association with overweight and obesity, low back pain, and diminished functional status. J Bone Joint Surg Am 93(7):662–670
13. Cheung KM, Samartzis D, Karppinen J, Mok FP et al (2010) Intervertebral disc degeneration: new insights based on "skipped" level disc pathology. Arthritis Rheum 62(8):2392–2400
14. Cheung KM, Karppinen J, Chan D, Ho DW et al (2009) Prevalence and pattern of lumbar magnetic resonance imaging changes in a population study of one thousand forty-three individuals. Spine 34(9):934–940
15. Scaal M (2016) Early development of the vertebral column. Semin Cell Dev Biol 49:83–91
16. Corallo D, Trapani V, Bonaldo P (2015) The notochord: structure and functions. Cell Mol Life Sci 72(16):2989–3008
17. Chan WC, Au TY, Tam V, Cheah KS, Chan D (2014) Coming together is a beginning: the making of an intervertebral disc. Birth Defects Res C Embryo Today 102(1):83–100
18. Rodrigues-Pinto R, Richardson SM, Hoyland JA (2014) An understanding of intervertebral disc development, maturation and cell phenotype provides clues to direct cell-based tissue regeneration therapies for disc degeneration. Eur Spine J 23(9):1803–1814
19. Risbud MV, Shapiro IM (2011) Notochordal cells in the adult intervertebral disc: new perspective on an old question. Crit Rev Eukaryot Gene Expr 21(1):29–41
20. Risbud MV, Schaer TP, Shapiro IM (2010) Toward an understanding of the role of notochordal cells in the adult intervertebral disc: from discord to accord. Dev Dyn 239(8):2141–2148
21. Fleming A, Keynes R, Tannahill D (2004) A central role for the notochord in vertebral patterning. Development 131(4):873–880
22. Bruggeman BJ, Maier JA, Mohiuddin YS, Powers R et al (2012) Avian intervertebral disc arises from rostral sclerotome and lacks a nucleus pulposus: implications for evolution of the vertebrate disc. Dev Dyn 241(4):675–683
23. Beckett MC, Ralphs JR, Caterson B, Hayes AJ (2015) The transmembrane heparan sulphate proteoglycan syndecan-4 is involved in establishment of the lamellar structure of the annulus fibrosus

of the intervertebral disc. Eur Cell Mater 30:69–88 **(discussion 88)**
24. Takahashi Y, Yasuhiko Y, Takahashi J, Takada S et al (2013) Metameric pattern of intervertebral disc/vertebral body is generated independently of Mesp2/Ripply-mediated rostro-caudal patterning of somites in the mouse embryo. Dev Biol 380(2):172–184
25. Adams MA, Dolan P (2012) Intervertebral disc degeneration: evidence for two distinct phenotypes. J Anat 221(6):497–506
26. Yin R, Lord EL, Cohen JR, Buser Z et al (2015) Distribution of Schmorl nodes in the lumbar spine and their relationship with lumbar disk degeneration and range of motion. Spine 40(1):E49–E53
27. Teraguchi M, Yoshimura N, Hashizume H, Muraki S et al (2015) The association of combination of disc degeneration, end plate signal change, and Schmorl node with low back pain in a large population study: the Wakayama Spine Study. Spine J 15(4):622–628
28. Walcott BP, Nahed BV, Mohyeldin A, Coumans JV, Kahle KT, Ferreira MJ (2012) Chordoma: current concepts, management, and future directions. Lancet Oncol 13(2):e69–e76
29. Choi KS, Harfe BD (2011) Hedgehog signaling is required for formation of the notochord sheath and patterning of nuclei pulposi within the intervertebral discs. Proc Natl Acad Sci U S A 108(23):9484–9489
30. Stafford DA, Brunet LJ, Khokha MK, Economides AN, Harland RM (2011) Cooperative activity of noggin and gremlin 1 in axial skeleton development. Development 138(5):1005–1014
31. Stafford DA, Monica SD, Harland RM (2014) Follistatin interacts with Noggin in the development of the axial skeleton. Mech Dev 131:78–85
32. Ellis K, Bagwell J, Bagnat M (2013) Notochord vacuoles are lysosome-related organelles that function in axis and spine morphogenesis. J Cell Biol 200(5):667–679
33. Buisson N, Sirour C, Moreau N, Denker E et al (2014) An adhesome comprising laminin, dystroglycan and myosin IIA is required during notochord development in Xenopus laevis. Development 141(23):4569–4579
34. McMillen P, Holley SA (2015) The tissue mechanics of vertebrate body elongation and segmentation. Curr Opin Genet Dev 32:106–111
35. Gray RS, Wilm TP, Smith J, Bagnat M et al (2014) Loss of col8a1a function during zebrafish embryogenesis results in congenital vertebral malformations. Dev Biol 386(1):72–85
36. Wilting J, Kurz H, Brand-Saberi B, Steding G et al (1994) Kinetics and differentiation of somite cells forming the vertebral column: studies on human and chick embryos. Anat Embryol (Berl) 190(6):573–581
37. Li D, Yang H, Huang Y, Wu Y, Sun T, Li X (2014) Lumbar intervertebral disc puncture under C-arm fluoroscopy: a new rat model of lumbar intervertebral disc degeneration. Exp Anim 63(2):227–234
38. Sakai D, Nishimura K, Tanaka M, Nakajima D et al (2015) Migration of bone marrow-derived cells for endogenous repair in a new tail-looping disc degeneration model in the mouse: a pilot study. Spine J 15(6):1356–1365
39. Kim KW, Kim YS, Ha KY, Woo YK et al (2009) An autocrine or paracrine Fas-mediated counterattack: a potential mechanism for apoptosis of notochordal cells in intact rat nucleus pulposus. Spine 30(11):1247–1251
40. Kim KW, Ha KY, Lee JS, Nam SW et al (2009) Notochordal cells stimulate migration of cartilage end plate chondrocytes of the intervertebral disc in in vitro cell migration assays. Spine J 9(4):323–329
41. Kim KW, Lim TH, Kim JG, Jeong ST, Masuda K, An HS (2003) The origin of chondrocytes in the nucleus pulposus and histologic findings associated with the transition of a notochordal nucleus pulposus to a fibrocartilaginous nucleus pulposus in intact rabbit intervertebral discs. Spine 28(10):982–990
42. Hunter CJ, Matyas JR, Duncan NA (2004) Cytomorphology of notochordal and chondrocytic cells from the nucleus pulposus: a species comparison. J Anat 205(5):357–362
43. Thompson K, Moore S, Tang S, Wiet M, Purmessur D (2018) The chondrodystrophic dog: a clinically relevant intermediate-sized animal model for the study of intervertebral disc-associated spinal pain. JOR Spine 1(1):e1011
44. Cai F, Wu XT, Xie XH, Wang F et al (2015) Evaluation of intervertebral disc regeneration with implantation of bone marrow mesenchymal stem cells (BMSCs) using quantitative T2 mapping: a study in rabbits. Int Orthop 39(1):149–159
45. Samartzis D, Borthakur A, Belfer I, Bow C et al (2015) Novel diagnostic and prognostic methods for disc degeneration and low back pain. Spine J 15(9):1919–1932
46. Peng B, Hou S, Wu W, Zhang C, Yang Y (2006) The pathogenesis and clinical significance of a high-intensity zone (HIZ) of lumbar intervertebral disc on MR imaging in the patient with discogenic low back pain. Eur Spine J 15(5):583–587
47. Shi R, Wang F, Hong X, Wang YT et al (2015) The presence of stem cells in potential stem cell niches of the intervertebral disc region: an in vitro study on rats. Eur Spine J 24(11):2411–2424
48. Henriksson H, Thornemo M, Karlsson C, Hägg O et al (2009) Identification of cell proliferation zones, progenitor cells and a potential stem cell niche in the intervertebral disc region: a study in four species. Spine 34(21):2278–2287
49. Li Z, Peroglio M, Alini M, Grad S (2015) Potential and limitations of intervertebral disc endogenous repair. Curr Stem Cell Res Ther 10(4):329–338

Affiliations

Feng Wang[1,2] · Cong Zhang[1,2] · Arjun Sinkemani[1,2] · Rui Shi[1,2] · Zhi-Yang Xie[1,2] · Lu Chen[1,2] · Lu Mao[1,2] · Xiao-Tao Wu[1,2]

✉ Xiao-Tao Wu
wuxiaotaospine@163.com

Feng Wang
wangfengspine@163.com

Cong Zhang
429063352@qq.com

Arjun Sinkemani
sinkemani@hotmail.com

Rui Shi
shiruiseu@163.com

Zhi-Yang Xie
uranter@126.com

Lu Chen
chan_dr8891@163.com

Lu Mao
bobai0008@163.com

[1] Department of Spine Surgery, Zhongda Hospital, School of Medicine, Southeast University, 87# Dingjiaqiao Road, Nanjing 210009, China

[2] Surgery Research Center, School of Medicine, Southeast University, 87# Dingjiaqiao Road, Nanjing 210009, China